SUPPLEMENT

Two sections within

1: Tables of MDE analysis Tables of MDE analysis for GBIF & CeDAMar, which list regression values for class replicates for rarefied diversity to centroids distance.

2: Satellite altimetry error The global bathymetry data available is a compilation of actual measurements and satellite derived features, where satellite data is used to constrain interpolations of actual measurements for globally complete coverage (Smith & Sandwell 2004). Use of this data in analysis requires a basic understanding of data resolution and limitations. In particular using satellite data alone, in regions of limited ship based measurements, may fail to pick up small scale features in the abyssal depth range. To quantify what that error is, this section derives a numerical values based on an idealized assumption.

Table 1: MDE results per replicate - CeDAMar

Replicates sorted by province. P-values for regression slope significant for alpha of 0.10 are bolded, with associated replicates underlined. Slope is mean rarefied species diversity for increasing distance away from centroid. Number of sites is sites used in analysis per replicate. Columns 9-11 refer to statistical values for distances between sites.

Province	Class	Regression slope	Regression intercept	R squared	P value slope	P value intercept	Number of sites	Site range km	Median distance km	Standard deviation distance km
2	Asteroidea	0.00009	2.24619	0.00356	0.69694	0.00959	45	3781	3651	868
2	Hexactinellida	-0.00409	24.66238	0.21756	0.69108	0.67235	3	117	5659	66
2	Lingulata	-1.74E-20	1.00000	0.50298	0.67735	0.00000	17	3413	1888	1386
2	Gastropoda	-0.00050	7.58504	0.00636	0.50558	0.00507	72	5100	3652	823
2	Ophiuroidea	0.00008	1.33120	0.01055	0.39065	0.00001	72	4954	3293	1114
2	Adenophorea	0.00065	0.20211	0.20738	0.36413	0.93408	6	2677	3893	1092
2	Anthozoa	0.00066	2.25481	0.02523	0.24225	0.26776	56	4949	3657	929
2	Echiuroidea	-0.00031	2.48321	0.07102	0.20810	0.00756	24	2959	3656	707
2	Actinopterygii	0.00079	-0.46681	0.07253	0.17434	0.83161	27	2016	3654	520
2	Phascolosomatidea	0.00000	1.00000	0.50682	0.16939	0.00000	34	2446	3655	950
2	Pycnogonida	-0.00346	14.34236	0.11511	0.15530	0.11130	19	251	3652	60
2	Malacostraca	0.00023	2.88479	0.01917	0.10791	0.00000	136	5150	3295	1357
2	Maxillopoda	0.00069	-0.22549	0.09489	**0.05642**	0.85830	39	2755	3659	673
2	Sipunculidea	0.00020	1.22739	0.04029	**0.04007**	0.00015	105	3409	3655	911
2	Ascidiacea	0.00059	1.27335	0.06209	**0.00898**	0.06703	109	3409	3648	1085
2	Crinoidea	-9.08E-19	1.00000	0.50594	**0.00854**	0.00000	20	1430	3653	419
2	Bivalvia	0.00065	0.64503	0.16120	**0.00691**	0.46626	44	5151	3756	1573
2	Polychaeta	-0.00407	21.01559	0.33390	**0.00028**	0.00000	35	5148	3652	1429
2	Holothuroidea	0.00071	1.56339	0.18549	**0.00010**	0.00659	76	5100	3651	1236
2	Echinoidea	-0.00045	2.73445	0.98725	**0.00006**	0.00001	6	2258	3829	894
2	Cephalopoda	-2.97E-19	1.00000	0.00E+00	**2.43E-14**	2.87E-104	8	2123	3650	747
4	Scaphopoda	2.60E-19	1.00000	0.57980	0.83437	1.86E-185	15	199	1564	50
4	Gastropoda	-0.00063	3.81720	0.00666	0.67982	0.05761	28	1082	1312	423
4	Holothuroidea	0.00311	-3.00274	0.22403	0.16706	0.34360	10	484	1446	170
4	Anthozoa	0.00382	-4.97041	0.99946	**0.00027**	0.00042	4	196	1565	96
4	Malacostraca	-0.03660	63.44762	0.46356	**0.00005**	0.00000	29	1053	1558	350
4	Echinoidea	0.01444	-21.52985	0.99829	**4.09E-08**	5.63E-08	7	199	1560	74
4	Maxillopoda	0.72125	-452.48253	0.94691	**1.15E-09**	7.64E-09	15	91	773	46
4	Polychaeta	0.27558	-411.71260	0.97610	**1.41E-13**	3.02E-13	17	199	1564	47
4	Sipunculidea	0.00895	-12.99158	0.99620	**1.14E-14**	2.88E-14	13	199	1565	54
4	Bivalvia	0.09964	-154.59413	0.99339	**5.64E-20**	7.08E-20	19	199	1564	45
5	Gastropoda	-0.04313	72.21014	0.56490	0.45857	0.35903	3	354	1296	197
6	Bivalvia	0.00027	0.68457	0.09572	0.69061	0.64210	4	1325	2269	578
6	Ascidiacea	-0.00241	8.97719	0.11745	0.50606	0.35247	6	393	2516	156
6	Gastropoda	-0.00046	2.76387	0.11148	0.22389	0.00580	15	1886	2179	646
6	Pycnogonida	0.00379	-8.20101	0.59892	0.12459	0.18483	5	393	2515	207
6	Sipunculidea	0.00093	-1.34774	0.42150	0.11458	0.34183	7	381	2517	179
6	Holothuroidea	0.00951	-21.40112	0.73358	**0.02941**	0.04445	6	393	2516	156
6	Malacostraca	-0.01076	44.67835	0.51180	**0.00018**	0.00000	22	3351	2169	877
7	Malacostraca	0.07908	-473.59424	0.45168	0.21399	0.23463	5	251	6340	104
7	Gastropoda	-0.01945	128.64234	0.30342	0.12428	0.11366	9	143	6442	66
8	Ascidiacea	-0.00002	2.28360	0.00011	0.95386	0.00487	33	2892	2839	967
8	Anthozoa	-0.00007	1.67407	0.01035	0.63621	0.00083	24	2892	2855	896
8	Bivalvia	0.00759	-28.17154	0.84784	0.25510	0.28427	3	518	4353	296
8	Ophiuroidea	0.00098	-0.57963	0.39787	**0.00042**	0.41383	27	2892	2839	1027
8	Malacostraca	0.00111	-0.66422	0.42912	**0.00009**	0.35305	30	2892	2875	940
11	Maxillopoda	0.07475	-94.75352	0.06259	0.16728	0.29294	32	188	1669	33
11	Polychaeta	-0.01430	47.60809	0.31019	**0.00139**	0.00000	30	1756	1853	514
11	Malacostraca	0.01506	-22.74805	0.46078	**0.00019**	0.00178	25	366	2025	179
12	Malacostraca	0.00123	0.49853	0.01302	0.40677	0.91897	55	2524	3322	327
12	Polychaeta	-0.00266	19.68432	0.01834	0.33838	0.03596	52	1208	3322	157
12	Anthozoa	-0.00040	2.36803	1.00000	**0.00030**	0.00014	3	2524	3451	1457

Table 2: MDE results per replicate - GBIF

Replicates sorted by province. P-values for regression. slope significant for alpha of 0.10 are bolded, with associated replicates underlined. Slope is mean rarefied genera diversity for increasing distance away from centroid. Number of sites is sites used in analysis per replicate. Columns 9-11 refer to statistical values for distances between sites.

Province	Class	Regression slope	Regression intercept	R squared	P value slope	P value intercept	Number of sites	Site range km	Median distance km	STD distance km
1	Adenophorea	-0.00034	1.92479	0.37394	0.19708	0.02077	6	1376	2321	641
1	Bivalvia	0.01421	-10.47195	0.03678	0.71586	0.76122	6	37	880	14
1	Malacostraca	0.00356	-1.64896	0.16363	0.32021	0.57151	8	188	879	71
2	Bivalvia	0.00027	1.42597	0.02102	**0.06568**	0.00471	162	3166	3729	871
2	Malacostraca	0.00013	1.04888	0.01219	**0.09489**	0.00008	230	5256	3655	790
2	Adenophorea	-0.00004	1.41093	0.00484	0.64589	0.00000	46	2882	1887	1037
2	Arachnida	-0.00053	2.21446	0.93652	0.16215	0.07626	3	1521	2066	789
2	Ascidiacea	-0.00024	4.58382	0.00329	0.66340	0.01083	60	2966	3323	767
2	Demospongiae	-0.00030	2.01417	0.10416	0.43557	0.04708	8	2509	2175	853
2	Hexactinellida	0.00001	1.08220	0.00119	0.92978	0.01504	9	3454	2863	1099
2	Maxillopoda	0.00002	1.60506	0.00012	0.94216	0.04223	48	3129	3770	966
2	Phascolosomatidea	0.00012	0.70443	0.05873	0.15444	0.02656	36	2930	3669	682
2	Rhynchonellata	-6.95E-19	1.00000	0.42461	0.40472	0.00000	5	379	4039	156
2	Sipunculidea	0.00006	1.13960	0.00801	0.31506	0.00000	128	3347	3546	811
4	Adenophorea	-0.00736	16.01322	0.93886	**0.03105**	0.01918	4	818	1681	440
4	Ascidiacea	-0.00375	7.95723	0.25633	0.16430	0.04848	9	687	1312	235
4	Bivalvia	-0.00089	3.24158	0.00996	0.63501	0.21655	25	686	1317	163
4	Malacostraca	-0.00107	2.78637	0.04632	0.11809	0.00008	54	1326	773	307
4	Sipunculidea	0.00069	0.37188	0.04413	0.49091	0.77710	13	638	1259	166
5	Sipunculidea	-0.00086	1.96252	0.61636	**0.02099**	0.00044	8	961	1036	322
5	Ascidiacea	-0.00055	2.05963	0.01059	0.80837	0.42228	8	496	1050	181
5	Bivalvia	0.00103	1.02203	0.03318	0.59194	0.64447	11	905	1275	276
5	Malacostraca	-0.00063	2.17566	0.05695	0.19605	0.00010	31	1188	1035	344
6	Adenophorea	0.00095	-0.32390	0.59209	**0.00925**	0.68003	10	3486	2501	1185
6	Maxillopoda	0.00044	0.28959	1.00000	**0.00001**	0.00004	3	2264	1608	1307
6	Ascidiacea	0.00001	1.55049	0.00029	0.93699	0.00597	24	4900	2498	1405
6	Bivalvia	-0.00011	1.51191	0.01461	0.63285	0.02338	18	2581	2513	604
6	Demospongiae	-5.51E-20	1.00000	0.45566	0.42610	0.00000	6	4603	3350	1632
6	Hexactinellida	0.00004	1.03716	0.02272	0.56363	0.00059	17	4756	2621	1374
6	Malacostraca	-0.00002	1.44336	0.00246	0.73763	3.20E-09	48	6505	2187	1646
6	Sipunculidea	-0.00002	1.21776	0.00319	0.75865	1.02E-08	32	5156	2379	1463
7	Ascidiacea	0.00028	-0.19996	0.05363	0.37113	0.91367	17	1803	6061	509
7	Malacostraca	0.00017	-0.00093	0.06272	0.11909	0.99893	40	2038	6462	478
7	Rhynchonellata	0.00070	-3.55083	0.91346	0.19009	0.26698	3	2486	6930	1275
7	Sipunculidea	-0.00019	2.32920	0.03228	0.37980	0.08461	26	1463	6144	410
8	Bivalvia	0.00027	1.08704	0.14670	0.05878	0.09306	25	6046	4312	1905
8	Ascidiacea	-0.00005	1.87832	0.00716	0.50956	0.00000	63	5821	3615	1596
8	Demospongiae	0.00035	-0.11751	0.57151	0.24401	0.90393	4	2218	3788	1079
8	Hexactinellida	-0.00005	1.41275	0.03963	0.74823	0.11647	5	5081	4228	1845
8	Malacostraca	0.00005	1.23751	0.00540	0.68937	0.02415	32	5552	3820	1579
8	Sipunculidea	0.00004	1.04751	0.03301	0.31161	0.00002	33	5402	4808	1965
9	Rhynchonellata	0.00027	1.00880	0.47560	**0.00635**	0.01538	14	6363	3686	2432
9	Adenophorea	-0.00168	4.29887	0.01980	0.28359	0.00126	60	1486	759	193
9	Ascidiacea	-0.00002	1.32598	0.00796	0.65156	2.95E-09	28	5467	1015	1767
9	Bivalvia	-0.00001	1.46459	0.00032	0.93411	0.00010	24	6017	2182	2127
9	Demospongiae	-0.00033	2.18001	0.26562	0.29538	0.06642	6	1504	3022	558
9	Hexactinellida	-0.00007	1.19155	0.05207	0.43268	0.00001	14	2536	1368	860
9	Malacostraca	-0.00004	1.57067	0.00453	0.57420	2.16E-14	72	5952	938	1431
9	Maxillopoda	-0.00031	1.79736	0.02897	0.74716	0.19047	6	1463	904	590
9	Monoplacophora	-0.00004	1.14446	0.00438	0.78775	0.00001	19	1784	908	463
9	Sipunculidea	-0.00003	1.21269	0.00415	0.80589	0.00002	17	2428	946	922
10	Ascidiacea	-0.00016	1.68962	0.15277	0.23461	0.00195	11	4398	2842	1325
10	Bivalvia	0.00039	1.19590	0.02370	0.74175	0.59083	7	1655	1794	607
10	Demospongiae	-0.00154	3.90231	0.94074	0.15655	0.10731	3	598	1794	311
10	Malacostraca	-0.00006	1.48123	0.00661	0.78229	0.00996	14	3115	1946	836
10	Sipunculidea	0.00001	1.29908	0.00044	0.96840	0.19951	6	2176	3166	955
11	Bivalvia	-8.49E-21	1.00000	0.55675	0.91163	1.01E-47	5	4668	1274	1816
11	Hexactinellida	-0.00006	1.23292	0.01825	0.74975	0.01244	8	2710	1935	808
11	Maxillopoda	0.00659	-3.28422	0.30318	0.20025	0.75209	7	1858	1877	656
12	Bivalvia	0.00003	1.09519	0.00756	0.79933	0.06627	11	4746	3795	1371
12	Malacostraca	0.00001	1.14484	0.00230	0.77811	0.00000	37	5877	3258	1806
12	Maxillopoda	0.00007	2.87766	0.00265	0.88774	0.09931	10	4908	2180	1761
13	Bivalvia	0.00020	0.67467	0.21943	**0.00079**	0.00003	48	3834	2244	967
13	Hexactinellida	0.00058	0.27682	0.44467	**0.03520**	0.57913	10	2345	2065	778
13	Ascidiacea	0.00006	1.01417	0.01409	0.60835	0.00038	21	2366	1686	621
13	Demospongiae	3.02E-06	1.22567	0.00005	0.97687	0.00009	20	3247	2197	949
13	Malacostraca	-0.00004	1.91537	0.00037	0.85223	0.00027	96	3393	2254	730
13	Sipunculidea	0.00025	0.78223	0.08504	0.11791	0.03251	30	2838	2356	623
14	Maxillopoda	-0.00576	13.74871	0.23904	0.51108	0.31584	4	533	1434	225

Satellite altimetry error

Satellite altimetry measures the magnitude (given as gravitational units) and wavelength properties (spatial characteristics of target surface) of radar returns. This information is used to correlate ocean surface height and shape with topography below. This is caused by the gravitational pull of the mass of an undersea feature on the local ocean water mass. (See subsection 1.4.3; Satellite altimetry).

Satellite derived bathymetry does not have the geopositional errors nor coverages problems, of older ship-based data, but does have resolution limitations (Smith & Sandwell 2004; Figure 9). Since the satellite altimetry data was released into the public domain via military declassification in 1995 (Sandwell et al. 2001), its analysis and use in determining bathymetry has progressed rapidly. A variety of factors create resolution limitations in this data (Yale et al. 1998). Some factors relating to resolution, satellite track coverage, data correction, and sensor technology, are improving such that an ideal error could shortly be approached (Sandwell et al. 2013).

An idealized error is based on optimal measurement conditions and assumes only the physics of attenuation of the gravitational signal based on depth. No improvement in measurement technology or methods can address the loss of signal due to attenuation. Gravitational strength diminishes as a function of the distance between objects. As depth increases the gravitational signal decreases. This diminishes the resolution of observable topography as the magnitude of the gravitational signal (mGal) is positively related to the size of the feature. If all possible factors involved in the environmental corrections in altimetry are optimally achieved, than the gravitational error range is $+-1\,mGal$. The Gal is a unit of acceleration used in the science of gravimetry. Where, $1\,mGal = 1\times10^{-5}\,ms^{-1}$, as 1 Gal = 1 cm/s^2, and is approximately $1/1000$ of standard Earth gravity. Importantly mean sea surface height errors caused by a turbulent sea surface, can be corrected for by repeat satellite tracks with diverse orientation, and therefore are assumed to be optimized in the Ideal error.

Assuming error is parameterized, as above, or reduced in the environmental noise at the altimetry stage, the remaining error is located in the transfer function and the signal attenuation by depth. The transfer function utilized in SRTM30 PLUS varies spatially by inclusion of local filters for various isostatic mechanisms (Smith & Sandwell 1994), the gravitational models used improve every successive iteration of new SRTM PLUS versions, as they are corrected by inclusion of actual ship-based measurements and increased satellite swath coverage (Sandwell et al. 2014). Not addressed in this initial analysis is regional sedimentation, which affects the accuracy of gravity to topography conversion. This accuracy can be accounted for in location specific transfer functions (which have the range of zero to one in terms of correlation between gravity and topography) if they are calibrated with actual measurements of sediment cover at

subregional scales, and corrections as such are currently utilized in the global topography predictions (Smith & Sandwell 1997).

For this work the transfer function is assumed to have a 100% correlation, varying from actual correlations. This leaves resolution error to be described as function of attenuation of signal by increasing depth only. The resolution loss is for the width and height of an undersea feature, as a function of depth.

For the purposes of equating gravitational error to topographic features several assumptions and simplifications were made which make converting the $+-1\,mGal$ gravity error to topographic resolution more tractably. Only small scale topographic features (large scale topographic features include ridge systems, a small scale feature might be a single seamount within a ridge system) are of interest so a transfer function was utilized that was spatially invariant to isostatic compensation mechanisms which vary by crustal age and formation, and operate at larger wavelengths varying by region. Following a spatially invariant framework, no accounting for variation in sedimentation was made. Only loss of features due to resolution was considered.

The loss of resolution may be considered more important than increased noise, or not finding a feature, rather than a false feature. As such, the following analysis is interested in the error rate of false negative rather than false positive. Given that abyssal depths are the focus here, the loss of signal at abyssal and average ocean depths skews errors to be false negatives, as features will be underestimated due to signal attenuation. In practice signal attenuation can be accounted for in the topography transfer function, but noise does limit possible resolution, and no transfer function can account for positive height features which fall below a detection limit due to the 1 mGal error.

The following analysis does not account for depressions in in mean topography, nor gravitational noise, only those positive features that would be missed. It is useful for a basic understanding of the limitations of satellite altimetry, such as the loss in ability to detect abyssal hills and other small scale rugosity/topography features. The determination of this Ideal error ($E_{\mathbf{x}}$) gives a method to produce a numerical approximation of spatial error by adjusting a few easily obtained input parameters. It was undertaken in part as a first step towards creating a method for applying a standard error filter to global bathymetric data for future use in more focused biogeographic/macroecological study. This method also allows for any worker utilizing publicly available gridded bathymetric data, to apply a systematic error estimate to the data without needing to analyze raw satellite altimetry data.

Determination of Ideal error

The **Ideal error** equation ($E_{\mathbf{x}}$), is based on an simplified topographic feature with average ocean crustal density, in an approximately conical shape, with a perfect circular base. An empirical relationship of abyssal hill heights to widths (but not lengths), and a sinusoidal profile was adopted for the idealized feature's shape. These steps are a basic mathematical simplification,

which gives the base width (can be rearranged for height) of a hypothetical feature that would be missed with satellite altimetry given an average depth for a larger grid square, in an area of interest. No other information is needed.

For calculations of ideal gravitational error in bathymetry the following equations, unless otherwise stated, are from Smith & Sandwell (1994), Smith (1998), and Sandwell et al. (2001). (See appendices in **Sandewell2001**, for more on equations used.) Because there is not 100% similarity in the satellite altimetry literature for symbols used in equations, the reader should be vigilant in moving between the primary literature and this section.

In converting gravity anomalies to predicted topography workers employ two dimensional Fourier transforms of the spatial field data into the spectral domain. This transfer facilitates ease of analysis, as the calculations used for converting satellite radar altimetry measurements into gravity anomalies, become algebraic as opposed to a series of differential equations. It also allows, high, low, and passband filtering of gravity data (Sandwell & Smith 1997), and recombinations of longwave (including longwave data derived from other sources) and shortwave processed data to be gridded. Utilization of the spectral domain has been chosen to avoid assumptions on the characteristic wavelengths of signals (Fu & Cazenave 2001). Fourier transforms are from the spatial domain to the spectral domain, where in the spatial domain $\mathbf{x}$ is the x and y dimensions, (x,y) of a Cartesian gravity field, not to be confused with a specific location on the earth or geoid. In the spectral domain $\mathbf{k} = [k_x, k_y]$ in the wavenumber plane, the wavenumber (k) is related to the wavelength by $k_i = 2\pi/\lambda_i$. Importantly at small wavelengths, or spatial scales, the gravity anomaly can be considered a flat approximation of earth's surface, and spherical and harmonic complexities of calculating localized gravity anomalies can be ignored (Smith 1998). The flat earth approximation is implicit in the following equations.

Calculation of Ideal error (E_X)

The following is the derivation of the horizontal width scale Ideal error $E_{\mathbf{x}}$, at location $\mathbf{x}$ as described by $f(d,g)$. Where, d is regional depth, and g is the 1mGal gravity error. The predicted bathymetry from satellite altimetry derived gravity at a real location $\mathbf{x}$, coordinate point (x,y), is defined as:

$$b_p(\mathbf{x}) = p_l(\mathbf{x}) + S_t(\mathbf{x}) \times a_g(\mathbf{x}) \tag{1}$$

$b_p(\mathbf{x})$ = Predicted bathymetry.

$p_l(\mathbf{x})$ = Passband prediction and long-wavelength regional depth (spectral).

$S_t(\mathbf{x})$ = True scaling function (input parameter inclusive), gravity to topography transfer function, also known as admittance.

$a_g(\mathbf{x})$ = Downward continued gravity (attenuation based on depth).

In this framework the formula is not spatially invariant as $S(\mathbf{x})$ may go to zero based on sediment cover at $\mathbf{x}$ (Smith & Sandwell 1994), $p_l(\mathbf{x})$ becomes spatially invariant for the Ideal error, because only the short wave band is of interest, which excludes the longwave regional variation. (See Smith (1998); Figure 6, which demonstrates convergences of different isostatic transfer models ($S_t(\mathbf{x})$) at short wavelengths.) The above equation is simplified to a more ideal form below :

$$b_p(\mathbf{x}) = p(\mathbf{x}) + S(\mathbf{x}) \times a_g(\mathbf{x}) \tag{2}$$

Where, $p(\mathbf{x})$ = A passband prediction with no explicit wavelength cutoff, yet assumed to be smaller than affected by regional compensation mechanisms, and large enough such that noise is does not impact it.

$S(\mathbf{x})$= Invariant transfer function, ignoring variation in sedimentation, not spatially variable to lithosphere compensation mechanisms. As described above, workers assume that the geoid and topography are linearly related in the spectral domain (Fu & Cazenave 2001), so after Fourier transforms, into the spectral domain, the above equations become:

$$\hat{g}(\mathbf{k}) = f(k) \times \hat{h}(\mathbf{k}) \tag{3}$$

The explanation for this equation is given by Fu & Cazenave (2001); pg. 411 equation (13), in Smith & Sandwell (1994); pg. 21,807 equation (2), and in Appendix C of Sandwell et al. (2001); equations C1-C3. However, it is the explanation and form of equations 14-16 from Smith (1998) that is adopted here.

$\hat{g}(\mathbf{k})$ = The Fourier transform of the gravity anomaly at position $\mathbf{x}$.

$\hat{h}(\mathbf{k})$ = The Fourier transform of the height, above the local depth (d) of the topography at position $\mathbf{x}$. Given that $h << d$ in this setting, the first approximation of C1 fromSmith (1998)is utilized which gives:

$f(k)$ =$C \times exp(q)$. C is considered a constant (Bouguer constant) if no compensation mechanism is utilized, and $C = 2\pi G(\rho_c - \rho_w)$. G= the Newtonian gravitational constant, ρ_c is the underlying crustal density, and ρ_w is seawater density. Assumed to be spatially invariant here, but actual density values vary in a nonlinear fashion. This leaves $exp(q)$, to vary, and $exp(q) = exp[-2\pi d \backslash \lambda] = e^{(-2\pi d \backslash \lambda)}$. And $\lambda^{-1} = \sqrt{\lambda_x^{-2} + \lambda_y^{-2}}$ (Smith 1998), and if the assumption that $\lambda_x = \lambda_y$, so horizontal scales are equal, as in the base diameter of a conical feature. Then for the Ideal calculation : $\lambda_{width} = \lambda$:

$$f(k) = C \times e^{(-2\sqrt{2}\pi d/\lambda)} \tag{4}$$

It is not possible to solve for λ at a given depth and gravity anomaly, without knowing h, as mathematical they are independent. However at this step, it is possible to invoke a deterministic ratio between height and width scales from empirical data, as the Ideal error is interested in the small scale features of the ocean, and abyssal hills are considered the most pervasive small global feature (Goff et al. 2004). The literature contains ratios of abyssal hills width by height ratios, determined empirically. As such a simple inverse relationship is utilized from the published work, which was derived from a linear regression equation produced using ~ 400 empirical surveys. The authors give the number of sites, but indicate that not all values are published. (See Goff et al. (2004), as this includes geographic extent of several major field sites, see other publications by Goff for further information.) From Goff 2010; Equation 3, and Figure 10:

$$H_{rms}(\mathbf{x}) = \frac{5}{101}\lambda_{hw} - 60.9 \tag{5}$$

$\lambda_h w$ = Abyssal hill width.

H_{rms}= The abyssal hill root mean square height in meters as a function of wavelength in meters. The H_{rms} is useful as an integrated height measure of an ideal feature, if the feature is assumed to have a sinusoidal shape, then amplitude, or peak height is given by: $\sqrt{2} * H_{rms}$. To make solving the following equations more tractable using Mathematica the y intercept term was removed, given that actual abyssal hill width scales are in kilometers the likely error introduced by this approximation is considered acceptable.

If equations (2.5) and (2.4) are substituted into Equation (2.3) then the only unknown for a given depth becomes λ, as such the Ideal error $E_{\mathbf{x}}$ can be solved for λ as a $f(d)$ only. From Equation (2.3) $\hat{g}(\mathbf{k})$ and $\hat{h}(\mathbf{k})$ can be simplified to $g(\mathbf{x})$ and $h(\mathbf{x})$. By removing the Fourier transform term $exp[]$ from both sides giving:

$$g = C \times e^{(-2\sqrt{2}\pi d/\lambda)} \times \frac{5}{101}\lambda \tag{6}$$

g = The gravity anomaly, which is $1{\times}10^{-5}\, m/s^2$.

$C = 7.84165 \times 10^{-7}\, s^{-2} = (2\pi * 6.674 \times 10^{-11}\, m^3/kg * s^2) \times (1870\, kg/m^3)$

Where, $(1870\, kg/m^3) = (\rho_c - \rho_w)$ and $\rho_c = 2900\, kg/m^3$ and $\rho_w = 1030\, kg/m^3$ (Carlson & Raskin 1984; Smith 1998).

$$g/C = \frac{5}{101}\lambda \times e^{(-2\sqrt{2}\pi d/\lambda)} \tag{7}$$

Using the software *Mathematica 10.0* and the "Reduce function" the proceeding equation was rearranged for λ in terms of depth (constrained with logical parameters $\{d > 0 \,\&\, \lambda > 0\}$). Results did not differ from solving using wolfram's free online Mathematica portal, or the proprietary software:

$$\lambda_m = (8.88577\, d_m)/(F_w[(11564952\sqrt{2}\, d_m \Pi)/1489558387)]) \tag{8}$$

$F_w[z]$ =The Lambert W Function = Product Log Function= gives the principal solution for w in $z = w \times e^w$ and in this case $z = -0.0344946\, d$, for $d > 0 \,\&\, \lambda > 0$ (rounded). This is the $E_{\mathbf{x}}$ equation **(Ideal error**) (Figure 2.1).

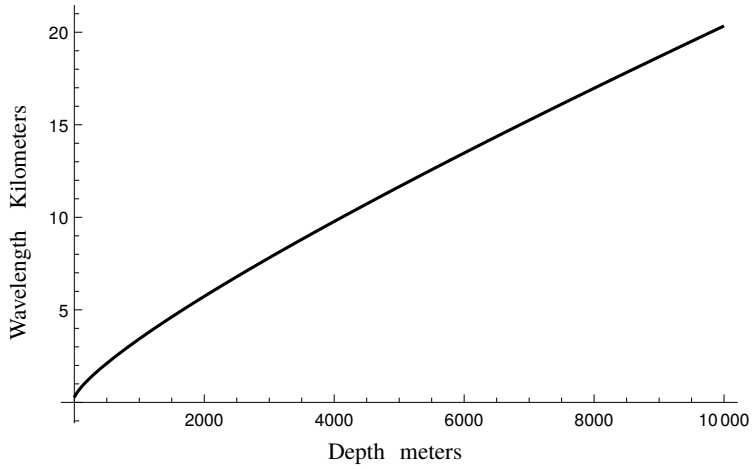

Figure 1: Ideal error - wavelength size by depth
Error width (λ) in kilometers. Depth is meters, 1-10,000 plotted. From Equation 2.8 Ideal error.

Equation 2.8 gives full wavelength (the horizontal scale of a feature), practically the Nyquist frequency most be taken into account. To avoid aliasing, any frequency must be measured at least twice per wavelength ($\lambda/2$). This becomes relevant for actual ship-based measurements to ground truth gravity width anomalies. The Ideal error assumes continuous satellite swath coverage, and so the Nyquist frequency does not directly affect the calculations above.

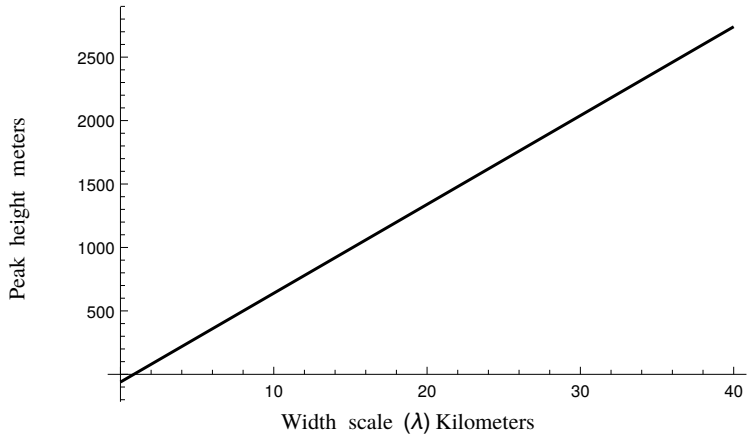

Figure 2: Ideal error - peak height by wavelength
Peak height as a function of horizontal width scale (λ) from the linear regression, Equation 2.5. Height in meters by width in kilometers is plotted from ~ 0 - 40. This range is two times greater than the Ideal error wavelength for a depth of 10 kilometers, see Figure 2.1.

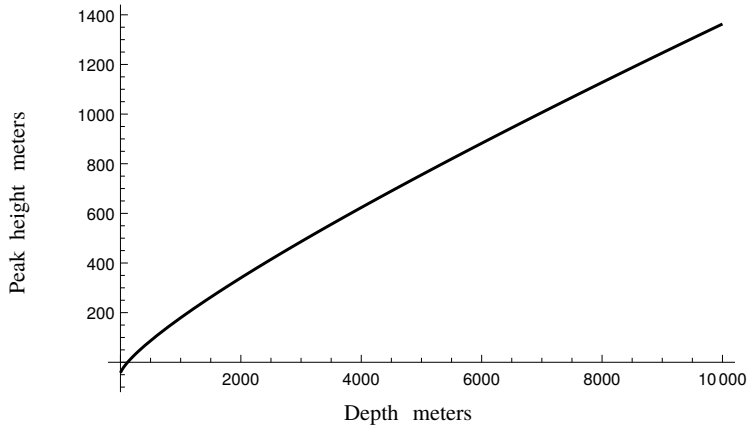

Figure 3: Ideal error - peak height by depth
Peak height as a function of depth, defined by the Error width scale at a given depth. Calculated by inputing Equation 2.8 into Equation 2.5. Negative values on the curve have no meaning.

The product of $E_{\mathbf{x}}$ equation, can be used to give an estimate of the peak height of a hypothetical missed feature. The sinusoidal Ideal peak height as function of wavelength at $\mathbf{x}$ is $\sqrt{2} \times H_{rms}(\mathbf{x})$, and $H_{rms}(\mathbf{x})$ is defined by combining Equations 2.8 and 2.5, which is plotted in Figure 2.2. Figure 2.3 is peak height plotted as a function of depth.

The $E_{\mathbf{x}}$ equation (2.8) was also calculated using the R statistical program (R Core Team 2014), version 3.1.2, using the package Lambert W version 0.6.4. The two programs (R & Mathematica) produced ~ 0.01 to 0.1 meter discrepancies in predicted wavelength when a non systematic comparison for abyssal depth values was undertaken. This error was considered

acceptable. This may be relevant as R is more heavily utilized by ecologists and biologists than Mathematica.

Incorporation of Ideal error

The Ideal equation was calculated to give a numerical approximation for spatial error in the bathymetric data used in creating abyssal province delineations. The figures within (Figures 2.1-2.3) may be compared with results in subsequent chapters and sections. As this may be a new method for determining error in satellite bathymetry data it might be useful for many unintended purposes. The equations for Ideal error features outlined here are simple enough, and can be applied to gridded modeled data without having to conduct analysis of raw satellite data. For example the current gravity anomaly data accuracy in polar regions is closer to $3 \times 10^{-5}\, m/s^2$ (Sandwell et al. 2013), which can be substituted into Equation 2.7 to produce a regional Ideal error. Similarly, seamount density values input into the C term of Equation 2.7, could be used for an $E_{\mathbf{x}}$ equation that is applied to resolution issues in detecting of Seamounts. The use of a conical sinusoidal simplification for shape of features is more applicable to seamounts than abyssal hills. Abyssal hills are formed as a series of ridges, and through a variety of processes (mass wasting, sedimentation, secondary crustal tectonics) become isolated hills. For this reason the length dimension regression to rms height shows no strong relationship (Goff et al. 2004). As such, the hypothetical feature should not be used to accurately represent the real shape of abyssal hills.

The location of ABS 3.0 boundaries need to be considered in the context of bathymetric accuracy errors. The upper depth bounds for abyssal provinces is 3500m. The peak height calculated for the Ideal error at a regional depth of 3500 meters is ~ 555 meters (with an ideal hypothetical feature of ~ 8.8 kilometers in base diameter). If this number is used as an approximate error for depth, errors in assumed bathymetry may have significant import on the location of province boundaries. Habitat heterogeneity at mid-ocean ridge boundaries likely being less well sampled by ships than continental margins. Importantly, the complex topography of the two major boundaries of most provinces are obscured by issues inherent in satellite altimetry. While the attenuation errors are more pronounced on the lower bounds, of the 6500 meter abyssal depth delineations, the limited relative coverage of trench areas globally, the higher use of ship-based measurements at those locations, and the greater slope of depth increase in those locations, make the Ideal error more applicable at upper bounds than the lower bounds of the abyss. The boundaries of abyssal provinces were calculated using an older version than the currently available global satellite derived bathymetry, and data quality should increase with each new release. It would be useful if methods used in creating boundaries were better known and publicly available, in order to update them with new bathymetric data and it's associated error. Additionally this would allow future incorporation of other BEPs, and biological data.

This section includes a hypothetical error, which warrants further investigation, in order for non-specialists to better utilize modeled global topography. Correlation of topography to gravity however relies on increased sampling (subsection 1.4.3; Satellite altimetry) , and regional values would need to be obtained from appropriate agencies and individuals. Resources listed prior give various estimates for the correlation of gravity to bathymetry, indicating a low correlation between topography and gravity anomalies at wavelength values similar to Ideal error width calculated here.

References

Carlson, R. L. & Raskin, G. S. (1984) Density of the ocean crust. *Nature*, **311**, 555–558.

Fu, L. & Cazenave, A. (2001) *Satellite Altimetry and Earth Sciences: A Handbook of Techniques and Applications*, Academic Press.

Goff, J. A., Smith, W. H. F. & Marks, K. M. (2004) The Contributions of Abyssal Hill Morphology and Noise to Altimetric Gravity Fabric. *Oceanography*, **17**, 24–37.

Goff, J. A. (2010) Global prediction of abyssal hill root-mean-square heights from small-scale altimetric gravity variability. *Journal of Geophysical Research: Solid Earth*, **115**, 1–16.

R Core Team (2014). *R: A Language and Environment for Statistical Computing*. Vienna, Austria.

Sandwell, D. T. & Smith, W. H. F. (1997) Marine gravity anomaly from Geosat and ERS 1 satellite altimetry. *Journal of Geophysical Research*, **102**, 10039.

Sandwell, D. T. et al. (2001) Bathymetry from Space: White paper in support of a high-resolution, ocean altimeter mission. *Int. Geophys. Ser*, **69**.

Sandwell, D. T. et al. (2014) New global marine gravity model from CryoSat-2 and Jason-1 reveals buried tectonic structure. *Science*, **346**, 65–7.

Sandwell, D. et al. (2013) Toward 1-mGal accurac y in global gravity from CryoSta2, Envisat, and Jason-1. *The Leading Edge*, **32**, 892–899.

Smith, W. H. F. (1998) Seafloor Tectonic Fabric From Satellite Altimetry. *Annual Review of Earth and Planetary Sciences*, **26**, 697–747.

Smith, W. H. F. & Sandwell, D. T. (1994) Bathymetric prediction from dense satellite altimetry and sparse shipboard bathymetry. *Journal of Geophysical Research*, **99**, 21803–21824.

Smith, W. H. F. & Sandwell, D. T. (1997) Global sea floor topography from satellite altimetry and ship depth soundings. *Science*, **277**, 1956–1962.

Smith, W. & Sandwell, D. (2004) Conventional Bathymetry, Bathymetry from Space, and Geodetic Altimetry. *Oceanography*, **17**, 8–23.

Wolfram Research, Inc. *Mathematica 10.0*.

Yale, M. M., Sandwell, D. T. & Herring, A. T. (1998) What are the limitations of satellite altimetry? *The Leading Edge*, 73–76.